FLUID-STRUCTURE INTERACTION ANALYSIS OF LARGE-BREAK LOSS OF COOLANT ACCIDENT

Tellervo Brandt[1], Ville Lestinen[1], Timo Toppila[1], Jukka Kähkönen[1],
Antti Timperi[2], Timo Pättikangas[2], Ismo Karppinen[2]

[1]*Fortum Nuclear Services Ltd, P.O.B .100, FI-00048 FORTUM, Finland*
[2]*VTT Technical Research Centre of Finland, P.O.B. 1000, FI-02044 VTT, Finland*

Abstract
In this article, we study a Large-Break Loss of Coolant Accident (LBLOCA) where a guillotine break of one of the main coolant pipes occurs near the reactor pressure vessel (RPV). This initiates a pressure wave which propagates inside the RPV. The simulation of bidirectional fluid-structure interaction phenomena has been found important for accurate prediction of the resulting deformation and loads. In this article, fully coupled simulation results are validated against the German HDR (Heißdampfreaktor) experiments. The computational fluid dynamic (CFD) software Fluent and Star-CD are applied to modeling of three-dimensional, viscous, turbulent fluid flow. The MpCCI code is used for bidirectional coupling of the CFD simulation to the structural solver Abaqus. Pressure boundary condition at the pipe break is obtained in a two-phase simulation with the system code APROS. Comparisons are made for break mass flow, wall pressure, displacement and strain. The simulation results follow the experimental data fairly well. In addition, the sensitivity of the results to numerical methods, grid resolution and pressure boundary condition are studied following the Best Practice Guidelines.

1. INTRODUCTION

Large-Break Loss of Coolant Accident (LBLOCA) is one of the design basis accidents of nuclear power plants (NPP). In a hypothetical accident scenario, a "guillotine" break of one of the main coolant pipes of the primary circuit causes a rapid pressure drop at the break location. The pressure transient propagates inside the reactor pressure vessel (RPV), and within the first hundreds of milliseconds after the break, the pressure loads induce deformations on the structures and threat their integrity. In this article, the pressure transient is simulated by coupling commercial computational fluid dynamic (CFD) and structural solvers using the MpCCI interface (MpCCI 3.0.6 Documentation 2007), The results are validated against the HDR (Heißdampfreaktor) experiments (Wolf 1981, Wolf 1982, Wolf *et al.* 1983), where LBLOCA was studied in a full-scale geometry by using realistic initial conditions. The main focus here is to validate a simulation environment which can be utilized in safety analysis of the Loviisa NPP which includes two VVER-440 type pressurized water reactors (PWR) owned by Fortum Power and Heat Ltd.

In earlier studies of pressure transient resulting from the pipe break during LBLOCA, accounting for bidirectional fluid-structure interaction (FSI) phenomena has been found important (see e.g. Wolf 1982, Anderson *et al.* 2003 and Lestinen *et al.* 2006). FSI simulation results obtained with bidirectional coupling of CFD and structural solvers have recently been validated against the HDR experiments by Anderson *et al.* (2003), Casadei and Potapov (2004) and Timperi *et al.* (2008). The HDR experiments and simulations with system codes like APROS (APROS The Advanced Process Simulation Environment) show that the FSI problem can be simulated as a one-phase flow approximately for the first 100 ms after the break (Wolf 1982, Timperi *et al.* 2008). However, two-phase phenomena have to be accounted for in evaluating the boundary condition at the break. Anderson *et al.* (2003) and Casadei and Potapov (2004) applied a finite-element based solver to account for inviscid fluid flow and structural motion. Timperi *et al.* (2008) compared the use of an acoustic model of water included in the structural solver to utilizing the Reynolds-Averaged Navier-Stokes (RANS) solver Star-CD (CD adapco Group 2004) for modelling of turbulent viscous fluid flow. They found that in the case of the HDR experiments, the latter approach was required. In the

present work, the CFD solver Fluent (Fluent 6.3 Documentation 2007) is applied together with the structural solver Abaqus (Abaqus/CAE 6.7 User Manual 2007), and the pressure at the break nozzle is taken from simulations with the system code APROS. The turbulent viscous fluid flow is simulated using the RANS approach as in the work of Timperi *et al.* (2008). The focus of the present work is in the sensitivity of the results to pressure boundary condition, numerical methods, grid resolution and turbulence modelling. The Best Practice Guidelines (Mahaffy *et. al* 2007) are followed as far as possible.

2. HDR BLOWDOWN EXPERIMENTS

The HDR blowdown experiments were carried out in the early 1980's in Germany. FSI phenomena caused by the flexibility of the core barrel during the initial depressurization phase of LBLOCA were studied in particular, and one of the main emphases was to provide reference data for validation of three-dimensional FSI codes.

The lay-out and the main dimensions of the test facility are shown in Fig 1. The break occurs in the nozzle A1 shown in Fig 1. Most of the other nozzles of the reactor were closed in order to provide clear boundary conditions for CFD calculations, and the effect of those left open was estimated to be small (Wolf 1981). The main parameters of the test facility are compared to those of Loviisa NPP in Table 1, and we see that the construction is quite realistic. However, a short break opening time, about 1 - 2 ms, was used in the experiments, whereas opening times of 10 - 15 ms or even longer have been proposed for a realistic break (Schall 1984, Anderson *et al.* 2003). The internals of the reactor were removed and their effect was simulated with a mass ring attached to the lower end of the core barrel. The lower end of the core barrel was free and the upper end was rigidly clamped.

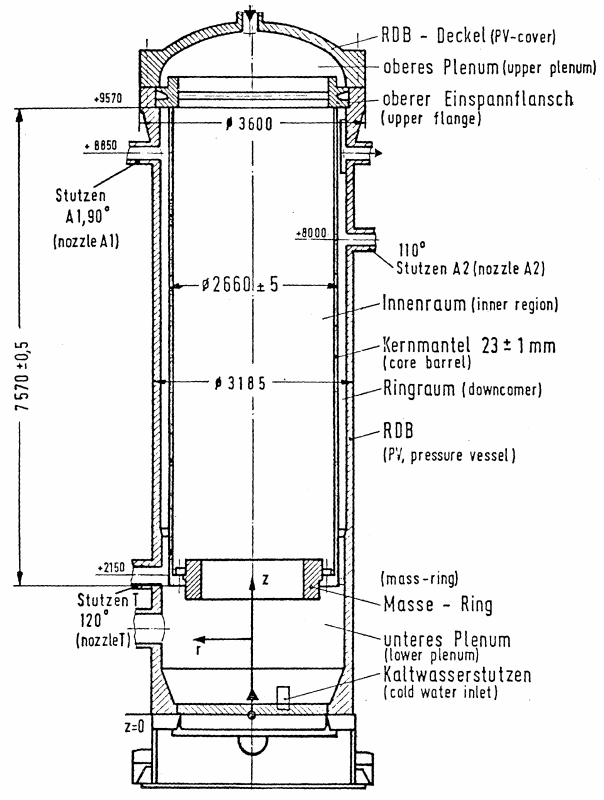

Fig 1 HDR reactor (Wolf et al. 1983).

Quantity	HDR	PWR
Pressure, MPa	11	12
$p_0 - p_{sat}$, MPa	5.5	7
$T_{core} - T_{downcomer}$, °C	0…50	30
Break diameter, m	0.2	0.5
Break opening time, ms	1…2	?
Core barrel length, m	7.6	8.1
Core barrel thickness, mm	23	50
Core barrel diameter, m	2.66	3.2
Maximum stress, MPa	100	230
Maximum displacement, mm	2	5

Table 1: Main parameters of the HDR blowdown experiments and Loviisa NPP.

Blowdown experiment V32, which was the base case in the experiment series, was chosen for this work. In this experiment, the downcomer and break nozzle temperature was 240 ºC and the core temperature varied axially from 308 ºC at the upper core to 283 ºC at the lower core barrel end.

Subcooling in the downcomer and break nozzle area was quite large in the experiment V32, i.e. 78 ºC which increased the loads on the core barrel.

3. NUMERICAL MODELS

3.1 Two-phase system code simulations

The system code APROS was utilized to evaluation of the pressure boundary condition for the CFD simulation. The APROS code calculated evaporation due to flashing and fluid acceleration inside the nozzle. Because small nodes were used in the calculation, critical flow model was not applied, and the flow was calculated directly with the conservation equations of mass, momentum and energy. The external pressure boundary for APROS calculation was adjusted with the measured pressure from the HDR experiment to get correct pressure reduction rate in the outlet of the nozzle, i.e. break opening time of 1 ms. Actual shredding out of the break disk was not simulated. Instead, a constant opening rate was assumed.

The break nozzle was modelled with 5, 15 and 45 nodes. To be able to provide a detailed time dependent pressure evolution during the first milliseconds after the break opening, the result from the case with 45 nodes was chosen as the CFD boundary condition. In this case, the node length in the break nozzle was 3 cm.

The pressure boundary condition for the CFD calculation was taken from a point inside the nozzle where there were not yet a significant void to allow single-phase CFD simulation. Pressure in this point using 5, 15 and 45 nodes in the nozzle is plotted on the left-hand side of Fig 2. In addition, pressure in the end of the nozzle is included from the case with 45 nodes and from the measurements. Pressure is depicted only for the first 0.01 s to show the details of the pressure drop. After t=0.01 s, pressure at the break location remains almost constant. The main difference between the APROS result and the measurement is the sharp drop of pressure when the break starts to open. The FSI-simulations were run both using the pressure boundary condition from the experiment and from the above described APROS simulation. Although the pressure drop is sharp in the APROS result, changing the boundary condition had only a small effect on the obtained pressure field and displacement.

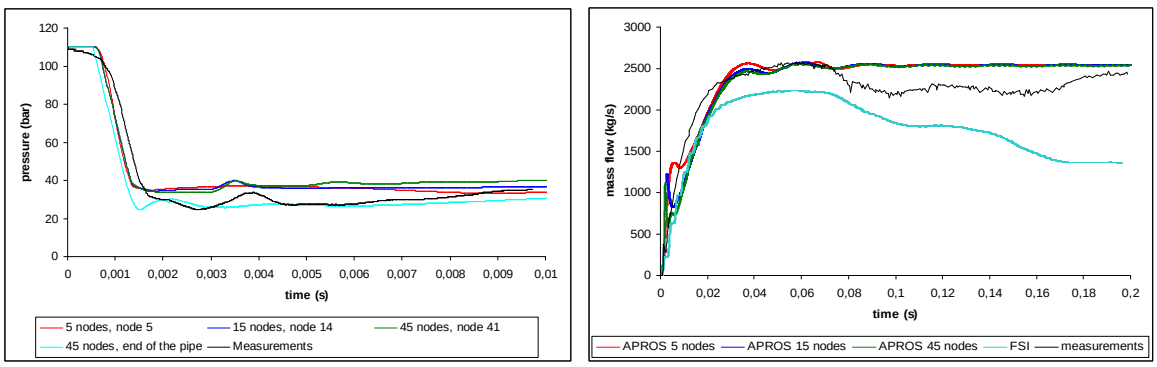

Fig 2: Comparison to experiments. Pressure boundary condition for the CFD model (left). Measured and calculated blowdown flow (right).

On the right-hand side of Fig 2, the calculated break mass flows obtained with 5, 15 and 45 nodes in the break nozzle are compared to experimental result. In addition, the mass flow from a fully coupled FSI-simulation is included. The FSI-result is somewhat below the experiments. The difference is mainly caused by the smaller density used in the FSI-simulation.

3.2 CFD model

Most of the simulations were performed with a CFD grid of approx 78000 grid cells. The grid is depicted in Fig 3 together with the model used in the structural solver. In the present flow case, the

emphasis is on capturing the pressure field, and the grid resolution is chosen accordingly. To study the sensitivity of the CFD results to the grid resolution, the resolution was first refined in the radial direction of the downcomer (120300 grid cells), and then also in the nozzle and in the nozzle joint area (124400 grid cells).

As can be seen from the experimental data, density and temperature remain almost constant during the first 0.20 s after the pipe break. Thus in the present simulations, a constant temperature was assumed. The simulations were repeated in three temperatures, in 308°C, 240°C which were the maximum and minimum temperatures in the experiment, and in 274°C which is the average of the two. The dynamic viscosity is approximately μ=0.0001Pa·s in these temperatures. Temperature has some affect on the obtained pressure fields, and here the results are presented for the 274°C case.

Fluent and Star-CD are both finite-volume based CFD solvers. In both codes, the pressure-based solver was utilized which is a standard choice in flows with low Mach number. The PISO pressure-correction method was applied. In the present application, water has to be treated as a compressible fluid. Thus, in the mass-balance equation, the non-constant density has to be accounted for, and this modifies the pressure-correction equation. In the pressure correction step, the correction of the mass flow, Δm, is written as

$$\Delta m = \Delta(A\rho u) = \rho\Delta(Au) + (Au)\Delta\rho \qquad (1)$$

where A is the cross-sectional flow area, ρ the density and u the flow velocity. The change of density, $\Delta\rho$, is evaluated using the change of pressure, Δp, and the compressibility of water, κ, as

$$\Delta\rho = \kappa\rho\Delta p \qquad (2)$$

The value for density is calculated using pressure as

$$\rho = \rho_0 + \kappa\rho_0(p - p_0) \qquad (3)$$

The applied reference values were ρ_0 = 758.5 kg/m^3, p_0 = 110 bar and κ= 1153.9e-12 Pa^{-1}. For more details on the pressure correction methods for compressible fluids see e.g. Ferziger and Perić (1999).

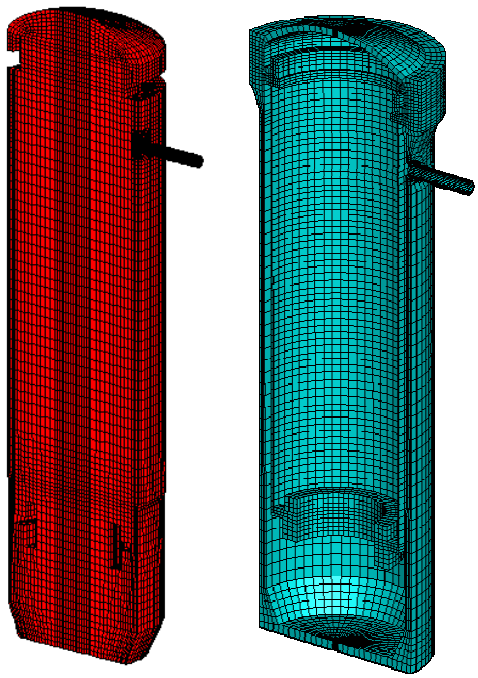

Fig 3: Computational meshes used in the CFD (left) and structural (right) models of the HDR reactor.

In the CFD model, solid walls were treated as viscous walls using wall functions. At the break nozzle, the pressure outflow condition was applied, and the static pressure obtained from the APROS simulation or from the experiment was set on this boundary.

In most of the simulations, the so-called standard k-ε turbulence model of Launder and Sharma with the standard wall functions was applied (Fluent 6.3 Documentation 2007). To study the effect of turbulence modelling, one simulation was run with the k-ω SST model using wall functions and one with no turbulence modelling.

The sensitivity of the obtained results to numerical methods was studied using Fluent. If the mesh is deformed, the first-order implicit time-integration method is the only available option in Fluent. Thus, the first-order method was used in simulations with bidirectional coupling, and both first and second-order methods were applied with one-way pressure mapping. In most of the simulations, the time step was set to 10 μs, which, in this case, corresponds to Courant number of 0.1 or below. In addition, some simulations were repeated using smaller and larger time steps. In most of the simulations, the number of iterations inside a time step was five. To ensure that the iteration was converged, the number of iterations was increased to seven and ten in some simulations.

The convective terms in the equations of momentum and turbulence quantities were discretized using the third-order MUSCL scheme of Fluent and the diffusion terms with a second-order central-difference scheme (see Fluent 6.3 Documentation 2007). Both second and first-order discretization was applied to pressure, but this did not affect the obtained pressure field.

In simulations using Star-CD, the Crank-Nicolson method was applied to the temporal discretization. For the spatial discretization, the Monotone Advection and Reconstruction Scheme (MARS) was used for velocities, central differencing for turbulence quantities and blended central-upwind differencing with blending factor 0.7 for density. (Timperi *et. al* 2008)

3.3 Structural model

In the finite-element based structural solver Abaqus, a linear finite-element model of the reactor with about 15000 8-node hexahedral elements was applied. Continuum shell elements, which have only displacement degrees of freedom but model shell behaviour accurately, were mainly used. Conventional solid elements were used in a few necessary regions. One layer of continuum shell elements was used in the core barrel wall and four layers in the RPV wall. The mesh of the structural model is shown in Fig 3. The structural model had a preliminary static load step in which the static pressure condition was achieved. After the static load step, applied pressure was provided by CFD code.

Material properties E = 175 GPa, ν = 0.3 and ρ = 7900 kg/m^3 were used for elastic modulus, Poisson's ratio and density of the core barrel, respectively. For the RPV, values E= 190 GPa, ν = 0.3 and ρ = 7850 kg/m^3 were applied. A small amount of stiffness proportional Rayleigh damping was included in the RPV wall. Value $\beta = 6\times10^{-6}$ was used which results in 2 % of critical damping at frequency 1000 Hz. The maximum frequency of interest was estimated as 400 Hz.

3.4 Coupling of CFD and structural models

The external coupling software MpCCI was applied to bidirectional coupling of the CFD and structural solvers. In this approach, the CFD and structural analysis codes run simultaneously and coupling information is exchanged during the simulation. Interpolation is used for transferring coupling quantities between the fluid and structure meshes. In this work, the coupling quantities were fluid pressure and nodal coordinates of the structure, and the codes exchanged information in the beginning of each time step. The simulations were run on a PC with Intell Core 2 CPU 1.86 Ghz processor in the Windows environment. A simulation for the time period $t=0$, …, 0.20 s took approximately 96 hours of wall clock time. The fully coupled simulation took approximately 33% more CPU time than a simulation with one-way pressure mapping. The increased computation is mainly caused by moving the RPV walls in Fluent, and communication between the codes does not seem to significantly increase the CPU time.

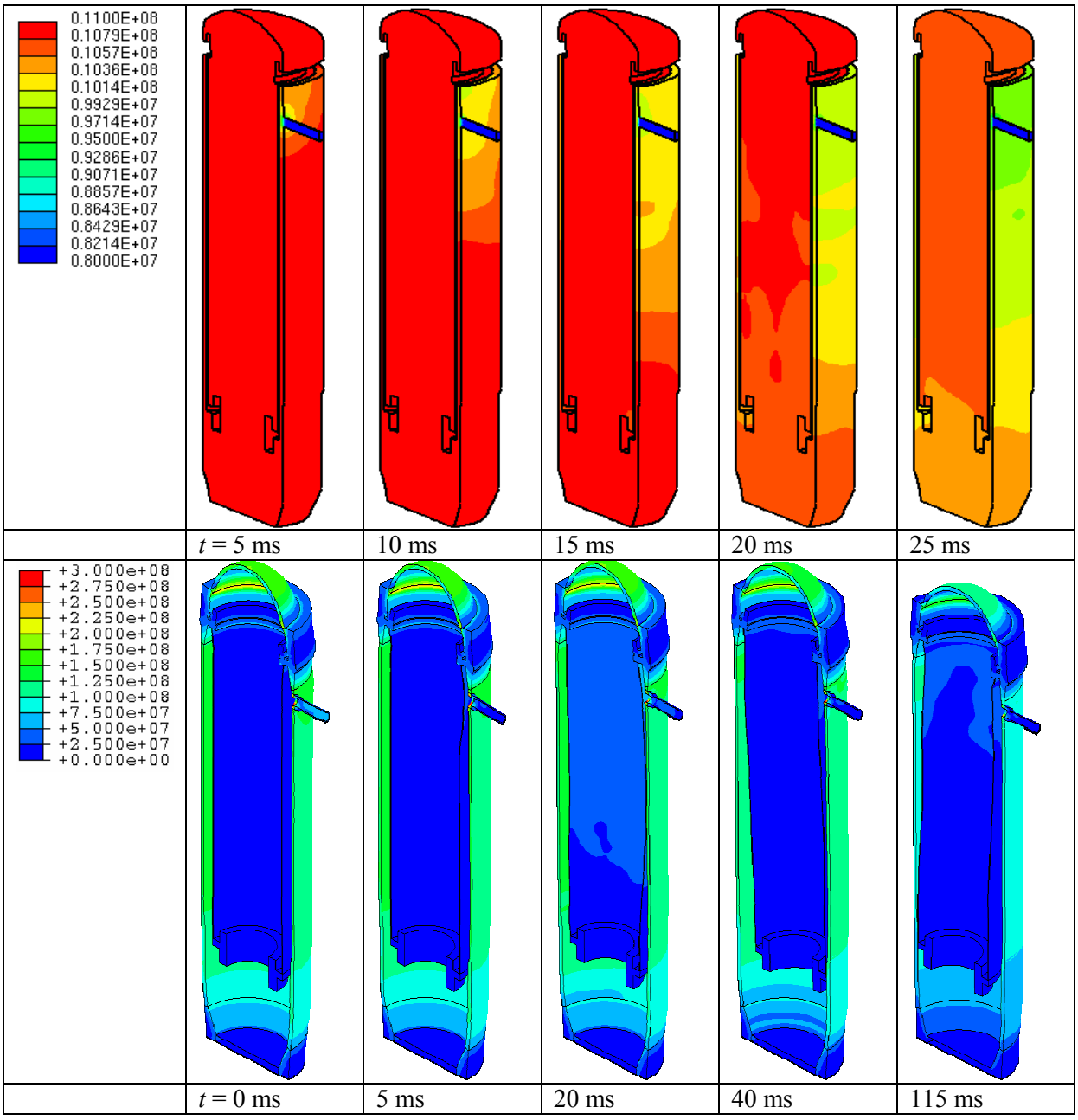

Fig 4: Pressure in the CFD model (upper). Von Mises stress, displacements are scaled with the factor of 200 (lower).

4 SIMULATION RESULTS

In this section, the FSI simulation results and their sensitivity to modelling related issues is discussed. In section 4.1, we start by comparing the present simulation results obtained with Fluent and Abaqus to experimental results and to the results of Timperi *et al.* (2008) which were obtained using Star-CD and Abaqus. The sensitivity of the results to time integration method, spatial discretization and turbulence modelling are studied in subsections 4.2-4.3, respectively. In addition in section 4.2, the necessity of using bidirectional coupling instead of one-way pressure mapping is demonstrated.

4.1 Bidirectional FSI simulations

In the cases discussed in this subsection, the coarser CFD grid depicted in Fig 3 was applied. The pressure boundary condition was taken from the APROS result and the k-ε turbulence model with wall functions was applied. The modeling details in Fluent and Star-CD were chosen as close to each other as possible, but as discussed in section 3.2, there were some differences in the numerical methods.

Propagation of the pressure wave and the resulting stresses and displacements are demonstrated in Fig 4. In the figures depicting the stress, the deformation is scaled by the factor of 200.

Pressure on the inner wall of the downcomer at the nozzle location (in cylindrical coordinates of Fig 1 at φ=90°, z=8.85m) and somewhat below the nozzle (φ=90°, z=2.3m) are depicted in Fig 5. Pressure on the opposite side of the downcomer (φ=270°, z=7.78m) is given on the left-hand side of Fig 6 and pressure on the core axis on the right-hand side of Fig 6. The pressure field is slightly underpredicted by both simulations, but it follows the experiments fairly well until approximately t=0.1 s. After this, flashing occurs (Wolf *et. al* 1983) and the one-phase model fails to describe the flow. During the first 20 ms, both simulations predict an oscillation of approximately 380 Hz in the pressure field. This frequency corresponds to a pressure wave travelling back and forth in the nozzle. This oscillation is not shown in the experiment which may be caused by boiling inside the nozzle (and outside it) which makes the water "soft" in this region.

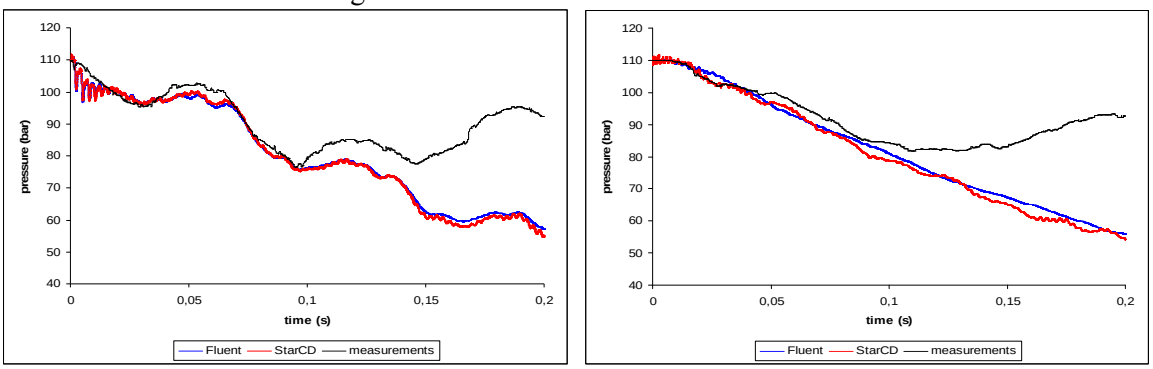

Fig 5: Pressure on the inner downcomer wall at φ=90°, z=8.85m (left), z=2.3m (right).

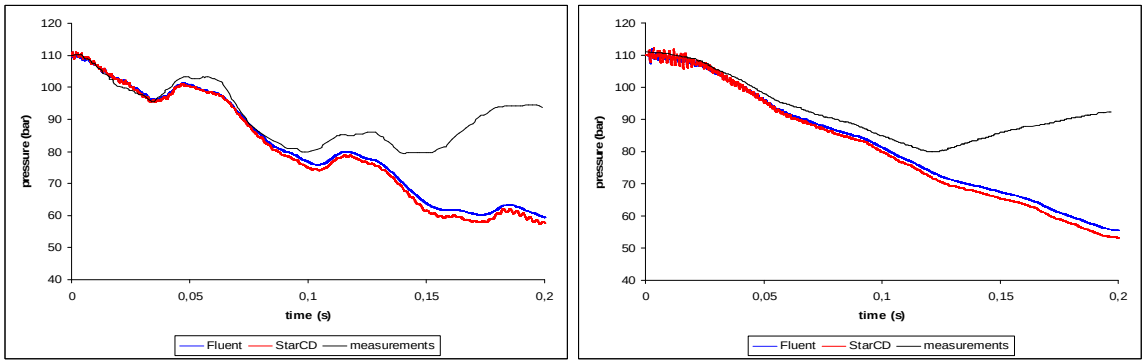

Fig 6: Pressure on the inner downcomer wall at φ=270°, z=7.78m (left) and on the core axis z=5.05m (right).

The pressure on both sides of the wall of the core barrel is underpredicted in a similar manner. Because of this, the pressure difference across the wall follows the experiment even better than the wall pressure. This is visible in the resulting relative displacements between the walls of the core barrel and RPV which are depicted on several locations of the downcomer wall in Fig 7-Fig 9. Here, we notice that the displacements are predicted fairly well for the entire duration of the simulations.

The Hoop strain and the axial strain on the wall of the core barrel are shown in Fig 10 and Fig 11. The strain oscillates with the frequency corresponding to the pressure wave travelling in the nozzle. This frequency was also visible in the pressure field. The result obtained with Star-CD oscillates clearly more than the one obtained with Fluent which is probably caused by different numerical methods.

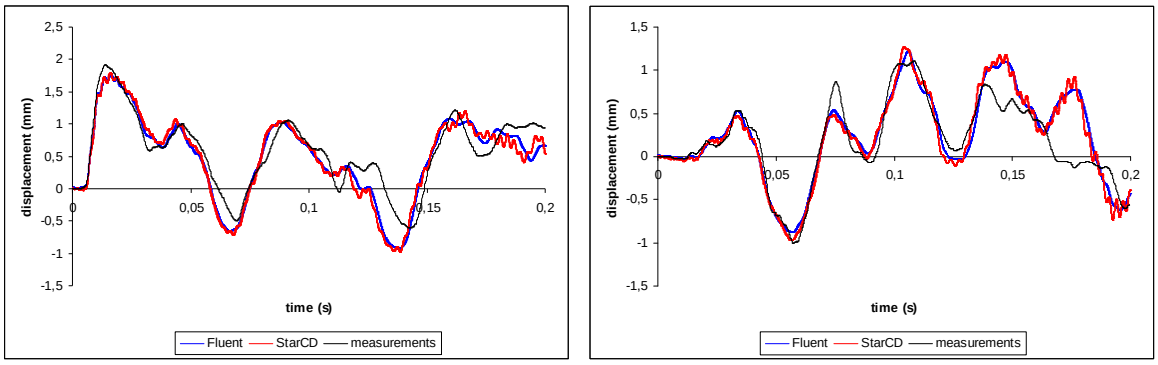

Fig 7: Relative radial displacement between the core barrel and RPV at z=7.15m, φ=90° (left) and φ=270° (right).

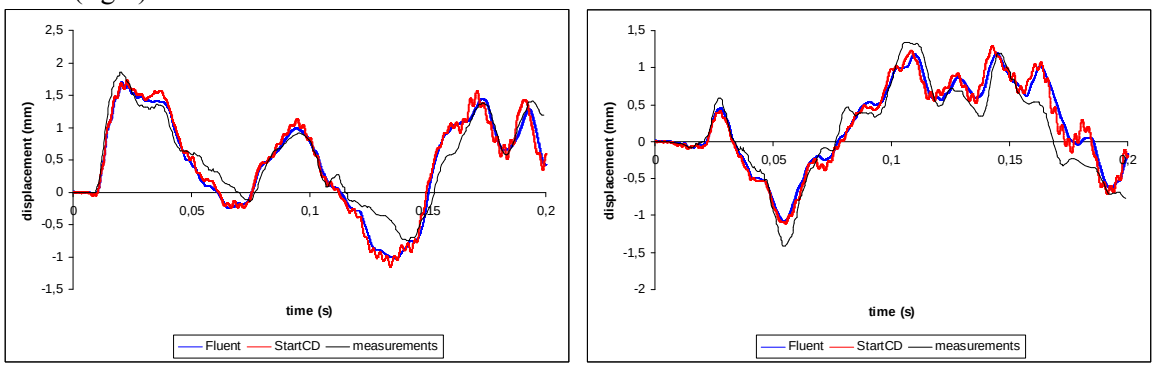

Fig 8: Relative radial displacement between the core barrel and RPV at z=5.55m, φ=90° (left) and φ=270° (right).

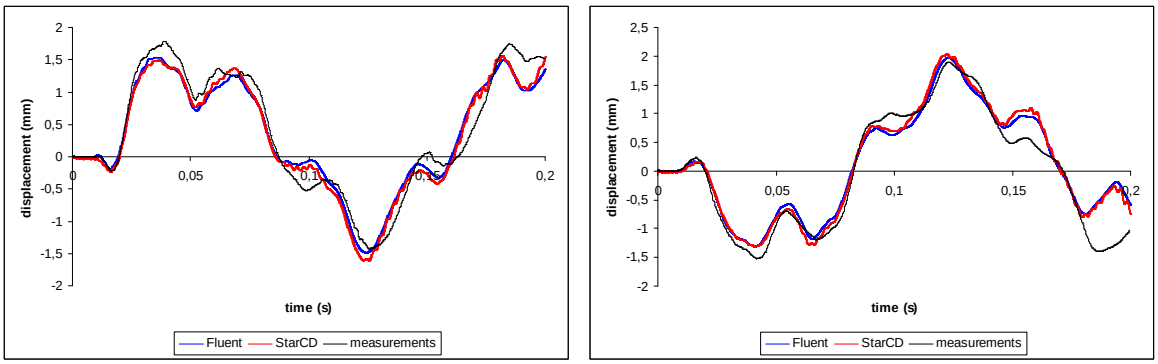

Fig 9: Relative radial displacement between the core barrel and RPV at z=2.3m, φ=90° (left) and φ=270° (right).

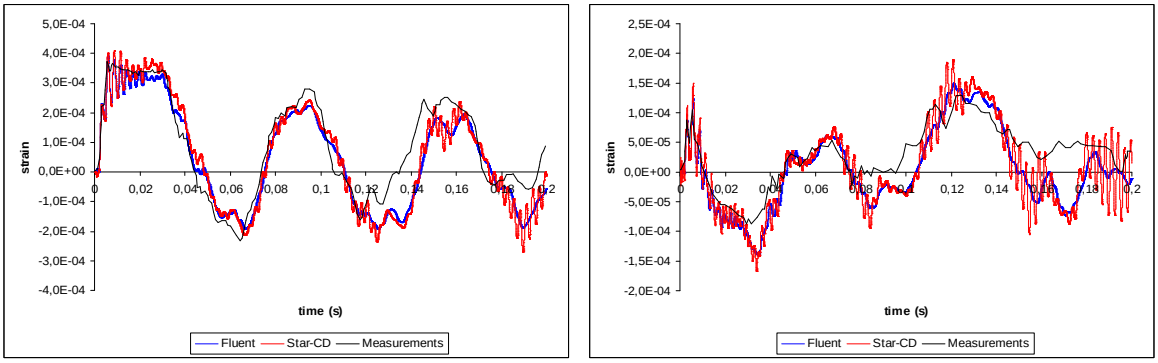

Fig 10: Hoop (left) and axial (right) strain on the outer surface of the core barrel at z=8.85, φ=90°.

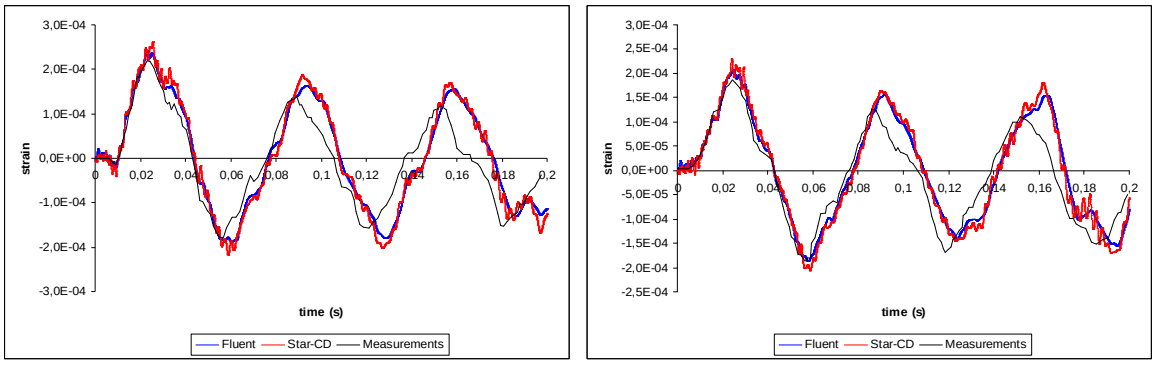

Fig 11: Hoop strain on the inner surface of the core barrel wall z=8.85, φ=135° (left) and at z=5.45, φ=225° (right).

The two CFD solvers produce almost identical results. However, the Fluent result is somewhat smoother. Since the same computational grid and pressure boundary condition were applied in the simulations with Fluent and Star-CD, the main difference between the two models is in the numerical methods. Based on the results of this subsection, we can conclude that the results are not strongly sensitive to numerical methods. The effect of numerics and discretization is studied more carefully in the following subsections.

4.2 Time-integration method with one-way mapping and bidirectional coupling

In Fluent, the first-order time-integration method is the only available option when the mesh is deforming. Because of this, the effect of the order of the time-integration method was studied using one-way pressure mapping where the walls of the CFD model remain rigid. These results also demonstrate the necessity of using bidirectional coupling. The pressure obtained using one-way pressure mapping, bidirectional coupling and measurements is depicted in Fig 12. In the fully coupled simulation, the wall movement damps the pressure oscillation. Displacement from fully coupled simulations and simulations with one-way pressure mapping are plotted in Fig 13. When the walls remain rigid in the CFD model and the pressure field does not react to the wall movement, the obtained displacements in the structural model differ considerably from the measurements. The differences between the one-way pressure mapping and bidirectional coupling are similar to those obtained by Anderson *et al.* (2003) who used a simpler model for the flow field.

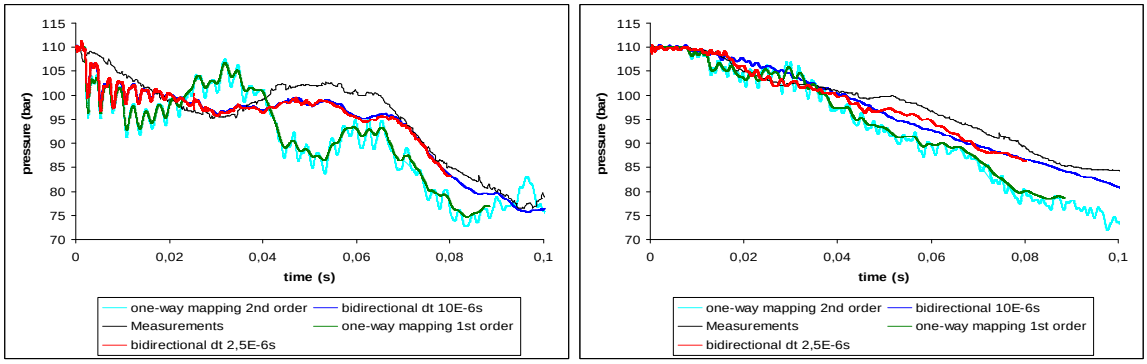

Fig 12: Effect of time integration method with one-way pressure mapping and bidirectional coupling. Pressure on the downcomer wall at z=8.85m, φ=90° (left) and at z=2.3m, φ=90° (right).

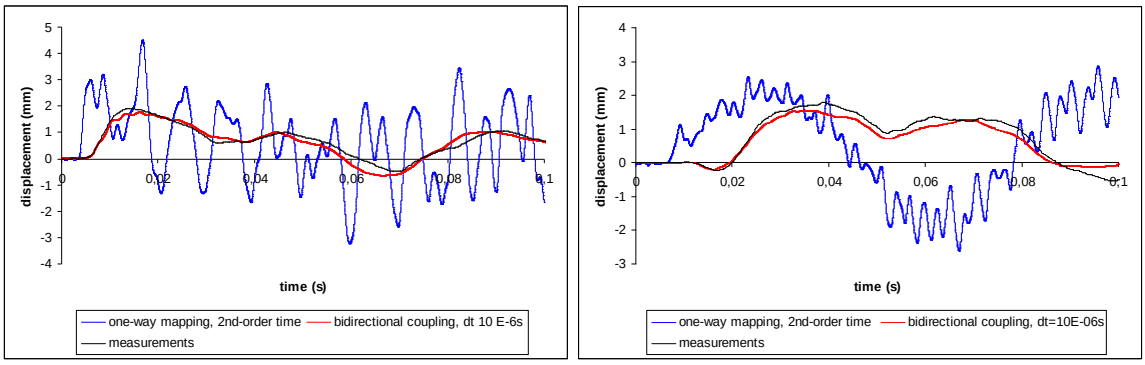

Fig 13: Effect of FSI. Relative radial displacement between the core barrel and RPV at z=7.15m, φ=90° (left) and at z=2.3m, φ=90° (right).

In Fig 12, we see that the order of the time-integration method affects the damping of the pressure fluctuation, but it has only a small effect on the general behaviour of the pressure field. In these simulations, the time step was 10 µs. Also the time step size was varied using the one-way mapping, and it turned out that in this case, the first-order method corresponds to the second-order method if the time step is one tenth of that used with the second order-method (not shown in the figure). In the simulations with bidirectional coupling, time steps of 10 µs and 2.5 µs were applied. We notice that some small pressure oscillations are not visible with the larger time step, but the overall behaviour is not strongly affected by the time step size. The simulations with the smaller time step are closer to the Star-CD where a second-order time-integration scheme was applied. The effect of time step size is most clearly visible in the strain which is depicted in Fig 14. In the previous section, we noticed that the strain obtained in the Fluent simulations oscillated less than the one obtained with Star-CD. Based on Fig 14, this is caused by the first-order time-integration scheme.

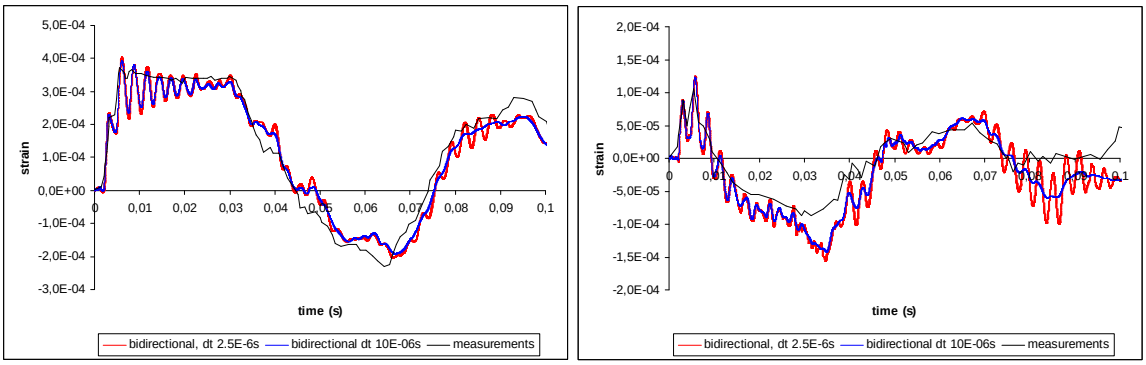

Fig 14: Effect of time step size. Hoop (left) and axial (right) strain on the outer surface of the core barrel at z=8.85, φ=90°.

4.3 Spatial discretization

The original grid resolution was mainly aimed at capturing the pressure wave and not to accurate description of the flow field. However, it was noticed by Timperi et al. (2008) that including a CFD model for the flow improved the results when compared to using the acoustic model. This suggests that also improved accuracy in the description of the flow field might affect the results. In the present work, the effect of grid resolution in the downcomer was considered as the restricting area of the original grid. The flow velocity is very low in most parts of the RPV, but especially near the nozzle, the velocity increases in the downcomer increasing also the resolution requirement. One simulation was performed with a tripled resolution in the downcomer (fine grid). After this, the resolution was increased also in the nozzle and in the nozzle joint area (fine grid 2). Pressure and displacement from the simulations with these three grids are plotted on the inner downcomer wall near the nozzle in Fig 15. We notice that increasing the grid resolution had only a small effect on the obtained pressure field and displacement, and thus the original grid resolution can be considered adequate.

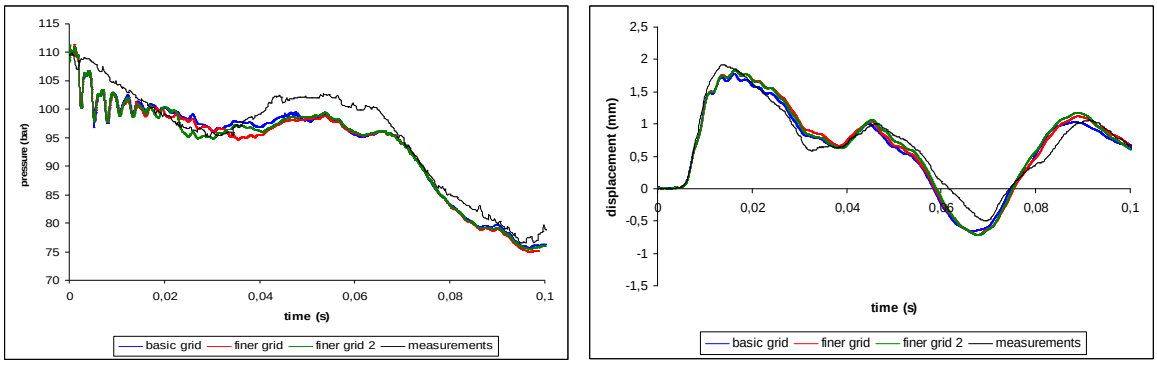

Fig 15: Effect of spatial discretization. Pressure on the inner downcomer wall at z=8.85m, φ=90° (left) and relative radial displacement between the core barrel and RPV at z=7.15m, φ=90° (right).

4.4 Effect of turbulence modeling

To study the effect of turbulence modeling, the simulation was run using two turbulence models, Launder-Sharma k-ε and k-ω SST, and with no turbulence modelling. In fully coupled cases, the k-ε model gave the best prediction for the pressure field. The results of the cases with k-ω and no modelling were very close to each other and they underpredicted the pressure field more than the k-ε model. This is demonstrated in Fig 16. The main difference between the two turbulence models was the turbulent viscosity for which the k-ε model gave much larger prediction than the k-ω model.

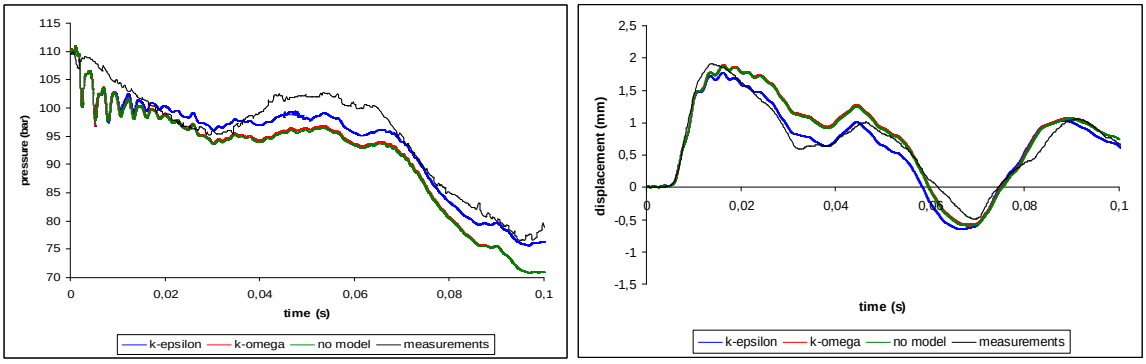

Fig 16: Effect of turbulence modelling. Pressure on the downcomer wall at z=8.85m, φ=90° (left). Relative radial displacement between the core barrel and RPV at z=7.15m, φ=90° (right).

5. CONCLUSIONS

In this article, we have presented results from simulations of the pressure transient occurring in the early phase LBLOCA. The results were obtained by bidirectional coupling of CFD and structural solvers. The pressure boundary condition was obtained in a two-phase system code simulation with APROS. The main aim of this work was to validate the simulation environment against the HDR experiments and to describe the sensitivity of the results to pressure boundary condition, numerical methods and grid resolution.

The assumption of one-phase flow used in the CFD model was valid until approximately t=100 ms and after this, the pressure field clearly deviated from the experimental result. During the first 100 ms, the obtained pressure field was slightly underpredicted, but it was still fairly close to the experiments. The pressure on both sides of the core barrel was underpredicted in a similar manner, and thus the pressure difference, which determines the wall movement, followed the experimental result even better. In addition, the pressure difference was not as sensitive to flashing as the wall pressure and the wall displacement was predicted quite accurately for the entire simulation, i.e. until t=200 ms.

The original CFD grid resolution and the time step were aimed at accurate description of the pressure wave. The sensitivity of the results to time step size, numerical methods, grid resolution and turbulence modeling was studied, and none of the variations clearly improved the original results.

However, there were some differences between the k-ε and k-ω turbulence models of which the k-ε model gave a better prediction. The reason for this is however unclear, because the grid was probably too coarse for accurate description of the flow field.

Based on the present results, we can conclude that the simulation environment is capable of simulating the FSI phenomena related to the early phase of LBLOCA where the flow can be considered as a one-phase flow. The obtained results were fairly close to experimental ones and they were not sensitive to pressure boundary condition, numerical methods or grid resolution, and thus it can be stated that the accuracy of the simulations was adequate.

ACKNOWLEDGEMENTS

This work was partly funded by the National Technology Agency of Finland (Tekes) within the MULTIPHYSICS project. This work is also a part of the SAFIR2010 programme (The Finnish Research Programme on Nuclear Plant Safety 2007-2010).

REFERENCES

Abaqus/CAE 6.7 User's manual, Dassault systems simulia corp. 2007

L. Andersson, P. Andersson, J. Lundwall, J. Sundqvist, K. Nilsson and P. Veber, "On the validation and application of fluid-structure interaction analysis of reactor vessel internals at loss of coolant accident", *Computers & Structures*, 81, 469-476 (2003).

APROS, The Advanced Process Simulation Environment, http://apros.vtt.fi/, Technical research centre of Finland

F. Casadei and S. Potapov, "Permanent fluid-structure interaction with non-conforming interfaces in fast transient dynamics", *Computer methods in applied mechanics and engineering*, 193, 4157-4194 (2004).

CD adapco Group, *Star-CD Version 3.20, Methodology* (2004).

J. H. Ferziger, M. Perić: "Computational Methods for Fluid Dynamics", 2nd edition, Springer, (1999).

Fluent 6.3 Documentation, User's guide, Fluent inc, 2007

V. Lestinen, T. Toppila, A. Timperi, T. Pättikangas and M. Hänninen, "Determination of thermal-hydraulic loads on reactor internals in a DBA-situation", *ASME Pressure Vessels and Piping Conference*, Vancouver, Canada, July 23-27 2006, PVP2006-ICPVT11-93456, (2006).

MpCCI 3.0.6-12 Documentation User manual, Fraunhofer Institute for Algorithms and Scientific Computing SCAI, Germany, 2007

J. Mahaffy, B. Chung, F. Dubois, F. Ducros, E. Graffard, M. Heitsch, M. Henriksson, E. Komen, F. Moretti, T. Morii, P. Mühlbauer, U. Rohde, M. Scheuerer, B. Smith, C. Song, T. Watanabe, G. Zigh, *Best practice guidelines for the use of CFD in nuclear reactor safety applications*, Nuclear energy agency committee on the safety of nuclear installations, OECD (2007)

M. Schall, "Untersuchungen von RDB-Einbauten bei Bruch einer Reaktorkühlmittelleitung", *HDR Sicherheitsprogramm, Technischer Fachbericht 48-84*, Kernforschungszentrum Karlsruhe. (1984)

A. Timperi, T. Pättikangas, I. Karppinen, V. Lestinen, J. Kähkönen and T. Toppila, "Validation of fluid-structure interaction calculations in a large-break loss of coolant accident", *Proc. of the 16th International Conference on Nuclear Engineering ICONE16*, Orlando, Florida, USA, May 11-15 2008, (2008).

L. Wolf, "Design report for the HDR-RPV-I blowdown experiments V31.2, V32, V33 and V34 with specifications for the pretest computation", *HDR Safety Program, Report No. 3.243/81*, Kernforschungszentrum Karlsruhe. (1981)

L. Wolf, "Experimental results of coupled fluid-structure interactions during blowdown of the HDR-vessel and comparisons with pre- and post-test predictions", *Nuclear Engineering and Design*, 70, 269–308 (1982).

L. Wolf, M. Schall, and H. Bader, "Untersuchungen von RDB-Einbauten bei Bruch einer Reaktorkühlmittelleitung", *HDR Sicherheitsprogramm, Technischer Fachbericht 29-82,* Kernforschungszentrum Karlsruhe. (1983).